MIMICKING BATS' ECHOLOCATION: A BIOMIMETIC APPROACH FOR INDOOR HUMAN TARGET DETECTION

Junkai Hou, Chunpeng Lu, Hanbin Guo, Yuan He*

Key Laboratory of Trustworthy Distributed Computing and Service, Beijing University of Posts and Telecommunications, Beijing, China
**yuanhe@bupt.edu.cn*

Keywords: DUAL-FREQUENCY RADAR SIGNAL, ELECTROMAGNETIC PROPERTIES, HUMAN TARGET DETECTION.

Abstract

In complex indoor environments, severe static clutter from indoor objects brings great challenges to human target detection, making the performance of existing clutter suppression methods not ideal. In this paper, we imitate the target discrimination method of bats, proposing a detection method for indoor human targets leveraging dual-frequency radar signal and electromagnetic properties. By analyzing the distinct power ratios of dual-frequency echoes, our approach classifies human targets and static clutter from the signal source rather than suppressing the existing clutter, solving the problem that existing clutter suppression methods do not perform well in complex indoor environments. Simulation results prove the effectiveness of this method.

1 Introduction

One major application for radar system is the detection of indoor human targets. However, radar clutter will decrease the detection capability of human targets by increasing the false alarm and miss rates, while submerging the target echo signal. As radar technology advances, clutter suppression approaches have progressively changed from conventional approaches like MTI and MTD to several novel techniques. For example, X. Wang et al. [1] introduced a deep learning cascade network based on residual network (VAE-ResNet) to suppress random clutter with enhanced feature extraction. A model based on GAN (Generation Adversarial Network) and GPCL (Gradient Point Clustering Localization) has been proposed to suppress clutter based on gradient point clustering algorithm [2]. Sparse Recovery-Based Space-Time Adaptive Processing (SR-STAP) has been proposed to leverage the sparsity of the clutter spectrum to enhance clutter suppression performance in bistatic radar systems [3]. Memory-Augmented Autoencoder-Based Nonhomogeneous Detector employs a memory-augmented autoencoder to enhance clutter suppression capabilities [4]. Instead of precisely detecting and categorizing echoes as clutter from the source, current clutter suppression strategies mainly focus on lessening the existing clutter signals' impact. Consequently, these techniques frequently encounter difficulties in successfully separating the intended object from a complicated clutter environment.

The presence of multiple reflection sources in the complex indoor environment results in a wider variety of echoes that radar receives, making it more difficult to distinguish human targets using the current clutter suppression approaches. Given the insufficiency of current approaches, our study leverages dual-frequency radar signal and electromagnetic properties to distinguish between targets and clutter from the source by simulating the natural sound patterns of bats. In Section 2, we provide a theoretical analysis in support of this. Section 3 presents the simulation experiments, Section 4 presents the discussion and the conclusion.

2 Modelling and Theory Analysis

As shown in Fig. 1, bat sonar can precisely detect small insect prey in the intricate jungle environment and has outstanding clutter-identifying capacity [5]. Bates et al. [6] clearly illustrated that bats can distinguish between prey targets and clutter by emitting signals of two different frequencies. [7] further demonstrated that bats can distinguish targets by comparing the power ratio of the two frequencies of echo signals from each target. The ability of bats to effectively distinguish targets from clutter in a complicated natural environment is quite similar to that of radar detection in a complex indoor environment. Hence, we distinguish indoor human targets by mimicking bat's echolocation pattern.

Fig. 1 Bats can accurately distinguish prey targets from other clutter targets in complex jungle environments.

As seen in Fig. 2, we constructed a simple indoor environment model that contains static clutter composed of the table and a

target to be identified composed of the human. The radar transmits signals with two frequency components f_1 and f_2 (assuming $f_1 < f_2$), mimicking the bat's echolocation pattern. We utilize $T(t)$ to symbolize the transmitted signal whose type is Ricker signal $R(f,t)$ which can be written as

$$R(f,t) = (1-2\pi^2 f^2 t^2) e^{-\pi^2 f^2 t^2} \quad (1)$$

so $T(t)$ can be expressed as

$$T(t) = R(f_1,t) + R(f_2,t). \quad (2)$$

According to the radar equation, the echo power of a single-frequency signal P_r can be expressed as

$$P_r = \frac{P_t G_t G_r \lambda^2 \sigma_{RCS}}{(4\pi)^3 R^4} \quad (3)$$

where P_t represents the power of the transmitted signal, G_t is the gain of TX antenna, G_r is the gain of RX antenna, λ is the wavelength of radar signal, σ_{RCS} is radar cross section (RCS), R is the distance between radar and target. Research [8] demonstrated unequivocally that RCS is correlated with frequency and material, primarily conductivity σ_{cond} and relative dielectric constant ε_r. Furthermore, RCS is also influenced by several variables, including target motion status, incidence angle, and target geometry [9]. RCS is exceedingly complex because of all these elements, so we mainly take frequency, conductivity and relative dielectric constant into account while assuming $G_t = G_r = G$, (3) can be rewritten as

$$P_r(f_i,\varepsilon_r,\sigma_{cond}) = \frac{P_t G^2 \lambda_i^2 \sigma_{RCS}(f_i,\varepsilon_r,\sigma_{cond})}{(4\pi)^3 R^4}. \quad (4)$$

Mimicking bats distinguish targets by comparing the power ratio of the two frequencies of echo signals, for a single target, its echo power ratio $P_{ratio}(\varepsilon_r)$ can be expressed as

$$P_{ratio}(\varepsilon_r) = \frac{P_r(f_2,\varepsilon_r,\sigma_{cond})}{P_r(f_1,\varepsilon_r,\sigma_{cond})} = \frac{\lambda_2^2 \sigma_{RCS}(f_2,\varepsilon_r,\sigma_{cond})}{\lambda_1^2 \sigma_{RCS}(f_1,\varepsilon_r,\sigma_{cond})} \quad (5)$$

considering

$$\lambda = \frac{c}{f} \quad (6)$$

so $P_{ratio}(\varepsilon_r)$ can be rewritten as

$$P_{ratio}(\varepsilon_r) = \frac{P_r(f_2,\varepsilon_r,\sigma_{cond})}{P_r(f_1,\varepsilon_r,\sigma_{cond})} = \frac{f_1^2 \sigma_{RCS}(f_2,\varepsilon_r,\sigma_{cond})}{f_2^2 \sigma_{RCS}(f_1,\varepsilon_r,\sigma_{cond})}. \quad (7)$$

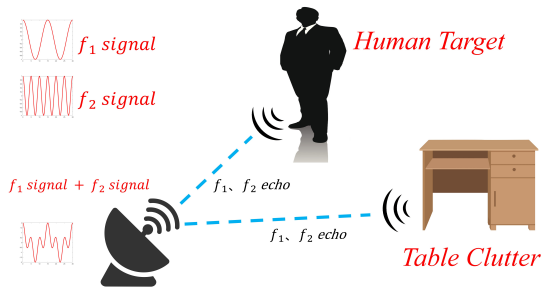

Fig. 2 Indoor environment model.

Since RCS depends on a wide range of variables, including frequency, angle, incident wave polarization, and others, no precise equations about RCS have been proposed so far, hence (7) cannot be further specified. To confirm that (7) may be utilized to distinguish human targets from other static clutter targets, we model different material targets with various electromagnetic properties using gprMax in Section 3.

3 Simulations and Results

3.1 Simulation Parameters Setting

Radar target detection can be divided into two main categories: single target detection and multiple target detection, so our simulation scenes also include the above two categories. The simulation results of indoor single-human targets are described in subsection 3.2, while the simulation results of indoor multi-human targets are described in subsection 3.3. These simulation experiments will demonstrate that human targets and table clutter can always be distinguished by (7), irrespective of the relative positions of the two and the number of human targets.

The electromagnetic properties of targets made of various materials vary, and the same target's electromagnetic properties will also vary with frequency. Data sheets of electromagnetic properties of wood and humans at different frequencies are provided in [10] and [11]. Following [10] and [11], Table 1 displays the simulation parameters of gprMax.

Table 1 Simulation Parameters of gprMax

Parameter	Value
Low frequency (f_1)	300 MHz
High frequency (f_2)	2400 MHz
ε_r of human in f_1	49.8
ε_r of human in f_2	38.1
ε_r of wood table in f_1	4.5
ε_r of wood table in f_2	3.5
σ_{cond} of human in f_1	0.641 S/m
σ_{cond} of human in f_2	1.44 S/m
σ_{cond} of wood table in f_1	0.005 S/m
σ_{cond} of wood table in f_2	0.023 S/m

3.2 Simulation of Single-human Target

3.2.1 Target and Clutter are in a Straight Line

Fig. 3 (Scene 1) shows the indoor single-human detection situations. The human target, radar, and table clutter are all in a straight line in scene 1, with (a) the human target in front of the table clutter and (b) the human target behind it. The simulation result of scene 1 is displayed in Fig. 4, while the results of scene 1(a) and scene 1(b) are displayed in Fig. 4(c) and 4(d), respectively. The simulation parameters of scene 1 are shown in Table 2.

(a)

(b)

Fig. 3. Scene 1: target and clutter are in a straight line, (a) shows the human target is in front of the table clutter, (b) shows the human target is behind the table clutter.

Table 2 Simulation Parameters of Scene 1

Parameter	Value
Distance from human target to radar in scene 1(a)	3.04m
Distance from table clutter to radar in scene 1(a)	6.02m
Distance from human target to radar in scene 1(b)	6.02m
Distance from table clutter to radar in scene 1(b)	3.04m

The simulation result of scene 1(a) is displayed in Fig. 4(c). The high-frequency signal's echo (2400MHz) is represented by the solid line, and the low-frequency signal's echo (300MHz) is represented by the dashed line. Since Fig. 4 shows the echo signals in the time domain, the two Ricker signal echoes on the left indicate the echoes of the human target because it is closer to the radar, while the two echoes on the right indicate the echoes of the table clutter. When we calculate the echo power ratio, we find that

$$P_{ratio}(\varepsilon_{r1}) = \left(\frac{27.48}{13.32}\right)^2 = 4.26$$

while

$$P_{ratio}(\varepsilon_{r2}) = \left(\frac{4.72}{3.11}\right)^2 = 2.30.$$

This indicates that the human target and table clutter can be distinguished from one another based on the echo power ratio value, since the human target's power ratio is higher than the table clutter's.

The simulation result of scene 1(b) is displayed in Fig. 4(d). The two Ricker signal echoes on the left in this scene represent the table clutter echoes, and the two Ricker signal echoes on the right represent the human target echoes because the table clutter is in front of the human target. When we calculate the power ratio, we find that

$$P_{ratio}(\varepsilon_{r1}) = \left(\frac{7.01}{3.30}\right)^2 = 4.51$$

while

$$P_{ratio}(\varepsilon_{r2}) = \left(\frac{21.17}{13.07}\right)^2 = 2.62$$

which means the power ratio of human target is also higher than the power ratio of table clutter, so human target and table clutter can also be distinguished.

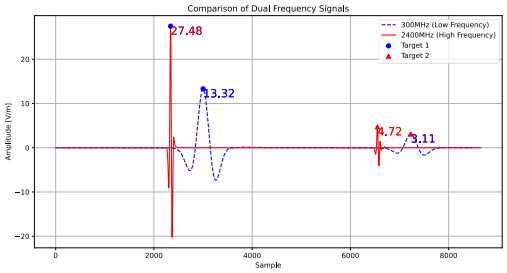

(c)

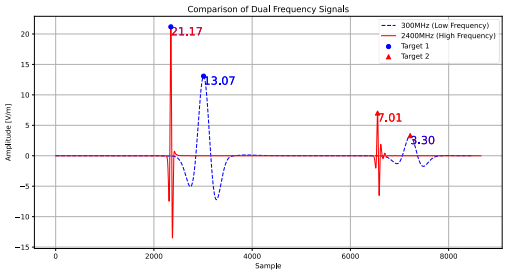

(d)

Fig. 4. Simulation result: (c) shows the result of scene 1(a); (d) shows the result of scene 1(b).

Through the simulation of scene 1, we find that when the human target and the table clutter are in a straight line, the echo power ratio of the human target is always higher than the echo power ratio of the table clutter regardless of whether the human target is in front of or behind the table clutter, so the two can be distinguished. In the next simulation experiments, we will prove that $P_{ratio}(\varepsilon_{r1}) > P_{ratio}(\varepsilon_{r2})$ also holds, so human target and table clutter can always be distinguished.

3.2.2 Target and Clutter are not in a Straight Line

Fig. 5 (Scene 2) also shows the scenario of indoor single-human detection. In scene 2, the human target and the table clutter are on the left and right sides of the radar. In this scenario, without loss of generality, the human target and table clutter are distributed on both sides of the radar at different azimuth angles and different distances, as shown in Fig. 5. More specifically, the distance between the table clutter and the radar is shorter than the distance between the human target and the radar.

Fig. 5. Scene 2: target and clutter are on the left and right sides of the radar.

Fig. 6 shows the simulation result of scene 2. The two Ricker signal echoes on the left represent the table clutter echoes, and the two Ricker signal echoes on the right represent the human target echoes. By calculating the power ratio, we find that

$$P_{ratio}(\varepsilon_{r1}) = \left(\frac{20.24}{9.49}\right)^2 = 4.55$$

while

$$P_{ratio}(\varepsilon_{r2}) = \left(\frac{29.91}{18.08}\right)^2 = 2.74$$

which means the power ratio of human target is also larger than the power ratio of table clutter, so human target and table clutter can also be discriminated. Simulation parameters of scene 2 are shown in Table 3.

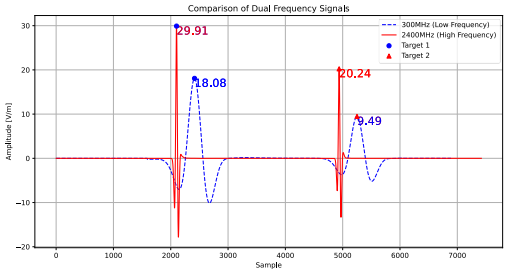

Fig. 6. Simulation result of Scene 2.

Through the simulation experiments of scene 1 and scene 2, we found that in the detection of single human target, no matter what the relative position of human target and table clutter is, $P_{ratio}(\varepsilon_{r1}) > P_{ratio}(\varepsilon_{r2})$ always holds true, so human target and table clutter can be discriminated.

Table 3 Simulation Parameters of Scene 2

Parameter	Value
Distance from human target to radar	3.91m
Distance from table clutter to radar	2.69m
The azimuth angle between human and radar	40°
The azimuth angle between table and radar	68°

3.3 Simulation of Multi-human Target

The indoor multi-human detection scene is depicted in Fig. 7 (scene 3). In this scenario, we have one table clutter and two human targets (human 1 is on the right, while human 2 is on the left). Each object's azimuth angle and distance from the radar vary from one another without sacrificing generality. Table 4 displays the scene 3 simulation parameters.

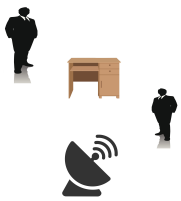

Fig. 7. Scene 3: multi-human detection.

The simulation result of scene 3 is displayed in Fig. 8. The three Ricker echoes are, in order, human 1, table clutter, and human 2, with human 1 being the closest to the radar, table clutter in the middle, and human 2 at the farthest. When we calculate the power ratio, we find that

$$P_{ratio}(\varepsilon_{r1,human1}) = \left(\frac{34.60}{16.19}\right)^2 = 4.57$$

$$P_{ratio}(\varepsilon_{r1,human2}) = \left(\frac{14.06}{6.66}\right)^2 = 4.46$$

while

$$P_{ratio}(\varepsilon_{r2}) = \left(\frac{15.79}{9.91}\right)^2 = 2.54.$$

Table 4 Simulation Parameters of Scene 3

Parameter	Value
Distance from human 1 to radar	2.39m
Distance from human 2 to radar	6.11m
Distance from table clutter to radar	4.00m
The azimuth angle between human 1 and radar	33°
The azimuth angle between human 2 and radar	31°
The azimuth angle between table and radar	0°

This indicates that two human targets can be distinguished from table clutter since their power ratios are almost equal, and both are greater than the power ratio of table clutter.

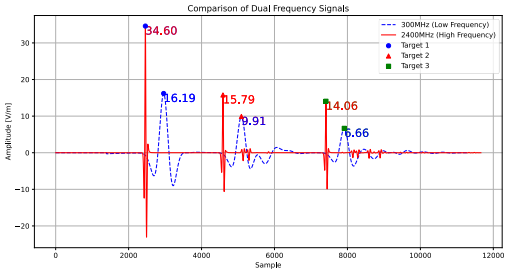

Fig. 8. Simulation result of scene 3.

Through the simulation of scene 3, we find that when the human target and the table clutter are not in a straight line and are no longer a single human target in the scenario, the echo power ratios of the two human targets are nearly the same, also higher than the echo power ratio of the table clutter, so the human target and table clutter can be distinguished.

3.4 Summary of Simulation Results

Based on the three simulation experiments mentioned above, we may conclude that $P_{ratio}(\varepsilon_{r1}) > P_{ratio}(\varepsilon_{r2})$ is always valid, while $P_{ratio}(\varepsilon_{r1})$ and $P_{ratio}(\varepsilon_{r2})$ are stable within their respective numerical intervals, regardless of the relative positions of the human target and the table clutter, as well as the number of human targets, according to which human target and table clutter can be distinguished. Table 5 displays all of the simulation findings, listing $P_{ratio}(\varepsilon_{r1})$ and $P_{ratio}(\varepsilon_{r2})$ values in four simulation scenes.

Table 5 Summary of simulation results

Power ratio / Scene	Human $P_{ratio}(\varepsilon_{r1})$	Table Clutter $P_{ratio}(\varepsilon_{r2})$
Scene 1(a)	4.26	2.30
Scene 1(b)	4.51	2.62
Scene 2	4.55	2.74
Scene 3	4.57 4.46	2.54

4 Discussion and Conclusion

In complicated indoor situations, our work suggests a dual-frequency radar signal-based clutter suppression technique that successfully separates static table clutter from human targets. We confirm the discrimination effect under various relative placements and target counts using the single-target experiment from scene 1 and scene 2, while the multi-target experiment is from scene 3. The findings demonstrate that under the simulated scenarios, the human target's echo power ratio is higher than that of table clutter, meaning $P_{ratio}(\varepsilon_{r1}) > P_{ratio}(\varepsilon_{r2})$ holds, allowing for discrimination between the two, regardless of the relative positions of the human target and the table clutter, as well as the number of human targets. By separating targets from clutter at the source, this technology overcomes the drawbacks of conventional methods and provides increased accuracy for applications such as healthcare monitoring, smart home systems, and security surveillance. Multipath effects and environmental complexity are still problems, though. To improve real-world applicability, future research should concentrate on managing various types of clutter and streamlining signal processing.

5 Acknowledgements

This work was supported by Beijing Natural Science Foundation Undergraduate "Qi Yan" Program under grant QY24198 and National Natural Science Foundation of China General Program under grant 62271064.

6 References

[1] X. Wang and H. Liu, "VAE-ResNet Cascade Network: An Advanced Algorithm for Stochastic Clutter Suppression in Ground Penetrating Radar Data," IEEE Transactions on Geoscience and Remote Sensing, vol. 62, pp. 1-12, 2024.

[2] F. Hou, M. Fang, T. Xianghuan Luo, X. Fan and Y. Guo, "Dual-Task GPR Method: Improved Generative Adversarial Clutter Suppression Network and Adaptive Target Localization Algorithm in GPR Image," IEEE Transactions on Geoscience and Remote Sensing, vol. 62, pp. 1-13, 2024.

[3] W. Huang, T. Wang and K. Liu, "A Data and Model-Driven Clutter Suppression Method for Airborne Bistatic Radar Based on Deep Unfolding," Remote Sens, vol. 16, pp. 2516, 2024.

[4] B. Zou, X. Wang, W. Feng, F. Lu and H. Zhu, "Memory-Augmented Autoencoder-Based Nonhomogeneous Detector for Airborne Radar Space-Time Adaptive Processing," IEEE Geoscience and Remote Sensing Letters, vol. 21, pp. 1-5, 2024.

[5] Carrer. L and Bruzzone. L, "A bat inspired technique for clutter reduction in radar sounder systems," Image and Signal Processing for Remote Sensing, Vol. 10004, pp. 404-413, 2016.

[6] Mary E. Bates et al, "Bats Use Echo Harmonic Structure to Distinguish Their Targets from Background Clutter," Science, vol. 333, pp. 627-630, 2011.

[7] Carrer. L and Bruzzone. L, "Solving for ambiguities in radar geophysical exploration of planetary bodies by mimicking bats echolocation," Nature Communications, vol. 8, pp. 2248, 2017.

[8] A. Androne, R. D. Tamas and S. Tasu, "Influence of the Substrate Material on the Radar Cross Section of Square Loop Unit Cells for Frequency Selective Surfaces," in International Workshop on Antenna Technology (iWAT), Bucharest, Romania, 2020, pp. 1-4.

[9] R. E. Jarvis, R. G. Mattingly and J. W. McDaniel, "UHF-Band Radar Cross Section Measurements with Single-Antenna Reflection Coefficient Results," IEEE Transactions on Instrumentation and Measurement, vol. 70, pp. 1-4, 2021.

[10] Gabriel C, Compilation of the dielectric properties of body tissues at RF and microwave frequencies, London, UK: King's College of London, 1996.

[11] Torgovnikov Grigory, Dielectric Properties of Wood and Wood-Based Materials, Berlin, Germany: Springer-Verlag, 1993.